GEOPHYSICAL RESEARCH LETTERS, VOL. 34, L07803, doi:10.1029/2006GL028108, 2007

Early calibration problems detected in TOMS Earth-Probe aerosol signal

P. Kiss,[1] I. M. Jánosi,[1] and O. Torres[2,3]

Received 7 September 2006; revised 4 January 2007; accepted 6 March 2007; published 5 April 2007.

[1] TOMS (version 8) ozone and aerosol data are analyzed in order to extract characteristic temporal patterns on a near global scale. A clear annual cycle of the global average for the ozone is apparent in the measured intervals (Nimbus-7: 1978–1993, Earth-Probe: 1996–2005), however a similar initial periodicity disappears for the aerosol index in the Earth-Probe records. A detailed spectral analysis revealed significant asymmetries in the Nimbus-7 aerosol signal for the two hemispheres, which is not present in Earth-Probe data. The available record from the Ozone Monitoring Instrument (one and a half years) shows a return to the seasonal variability seen by Nimbus-7 in both hemispheres. This suggests that calibration difficulties of the Earth-Probe instrument started earlier than mid 2000, when it became apparent from many indications. **Citation:** Kiss, P., I. M. Jánosi, and O. Torres (2007), Early calibration problems detected in TOMS Earth-Probe aerosol signal, *Geophys. Res. Lett.*, *34*, L07803, doi:10.1029/2006GL028108.

1. Introduction

[2] Satellite instruments are the most effective way to achieve a global view of the atmosphere. The polar orbiting Total Ozone Mapping Spectrometers (TOMS) have been a successful series of instruments designed for measuring total column ozone (TO). Other well-known TOMS products are the aerosol index (AI), reflectivity, ultraviolet radiation, and volcanic SO_2 (http://toms.gsfc.nasa.gov/). The Ozone Monitoring Instrument (OMI), launched in July 2004 on the Aura Satellite is continuing the long-term record of these atmospheric observations,

[3] The TOMS Aerosol Index can be thought of as a measure of the accuracy of the forward calculations to explain the backscattered UV radiation field measured by the TOMS sensor relative to a pure Rayleigh scattering atmosphere. The radiative transfer model assumes a molecular atmosphere and an ozone profile, bounded at the bottom by a Lambert Equivalent Reflector. The AI is simply a residual parameter that quantifies the difference between the measured and the calculated radiances.

[4] Zero residues are produced when the radiative transfer processes accounted for in the forward model adequately explain the observations. Non-zero residues may result from either geophysical phenomena unaccounted for in the radiative transfer calculations, or instrumental effects generally associated with poor instrument characterization. In the absence of calibration difficulties, however, non-zero residues are produced solely by geophysical effects, of which absorbing aerosols are by far the most important source. Hence the term Aerosol Index has been coined to refer to this residual quantity. For historical reasons the AI is expressed in N-value units [*Herman et al.*, 1997]. In the version 8 definition a unit AI is equivalent to a 2.3% reflectance change at 360 nm relative to 331 nm. Details on the dependence of the AI on aerosol related parameters are available in the literature [*Herman et al.*, 1997; *Torres et al.*, 1998; *De Graaf et al.*, 2005].

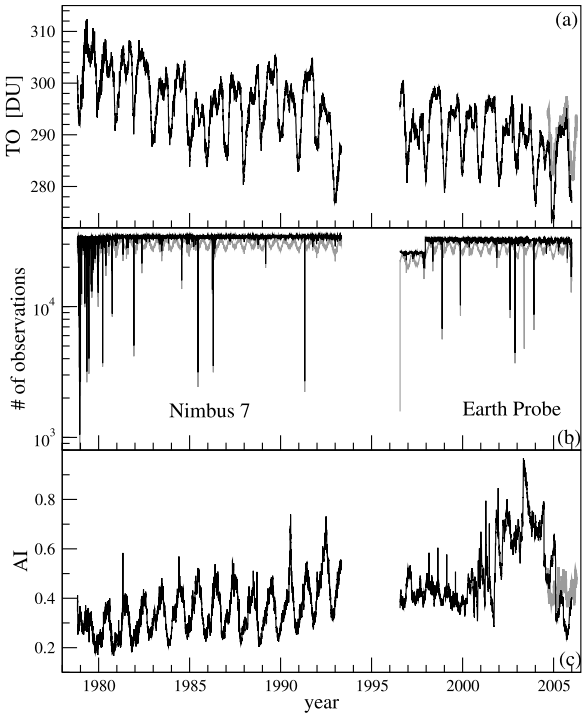

Figure 1. (a) Daily mean total ozone (in Dobson units) averaged over 60°S and 60°N for the TOMS (black) and OMI (gray) data. (b) Number of daily observations for the Nimbus-7 and Earth-Probe satellites in the band 60°S and 60°N (black: total ozone, gray: aerosol index; note the logarithmic vertical scale). (c) Daily mean aerosol index for the same geographic area, black/gray denote TOMS/OMI data. Only days of more than 20000 observations are included in the following periods: 11/01/1978–05/06/1993 (Nimbus-7), 07/25/1996–12/30/2005 (Earth-Probe), 09/06/2004–04/01/2006 (OMI).

[1]Department of Physics of Complex Systems, Loránd Eötvös University, Budapest, Hungary.
[2]NASA Goddard Space Flight Center, Greenbelt, Maryland, USA.
[3]Joint Center for Earth Systems Technology, University of Maryland Baltimore County, Baltimore, USA.

0094-8276/07/2006GL028108$05.00

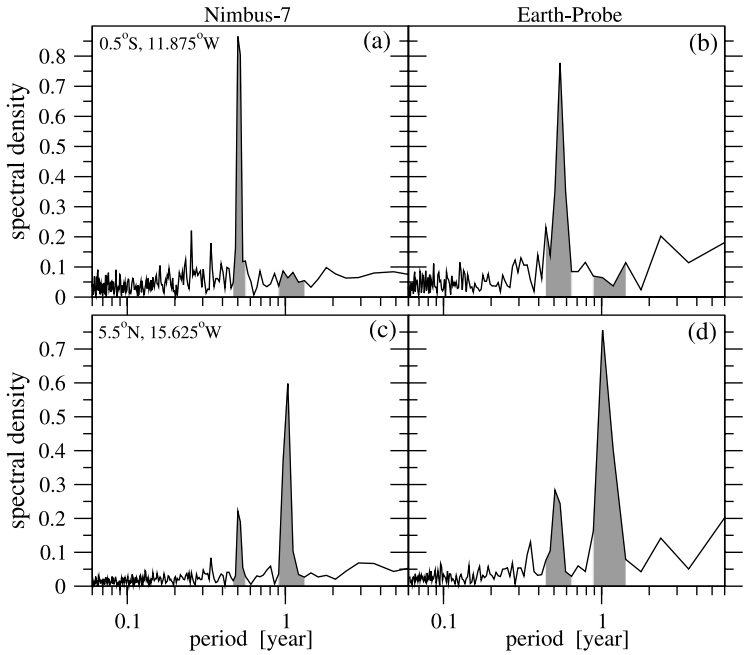

Figure 2. Normalized spectral densities as a function of period (note the logarithmic scale) for two geographic locations. (a) N7-AI, 0.5°S, 11.875°W. (b) EP-AI, the same location. (c) N7-AI, 5.5°N, 15.625°W. (d) EP-AI, the same location. Gray shading indicates the peaks for the semi-annual and annual spectral components.

[5] In this work we investigate the effect of instrumental calibration drift on the AI reported by the Earth-Probe TOMS sensor.

[6] The TOMS project has produced the longest available global record of aerosol observations in terms of AI. The TOMS AI record has significantly contributed to the present understanding of aerosols spatial and temporal distribution. Global sources of atmospheric soil dust have been identified [e.g., *Herman et al.*, 1997; *Israelevich et al.*, 2002; *Prospero et al.*, 2002; *Torres et al.*, 2002;], extreme episodes such as forest fires [e.g., *Hsu et al.*, 1999; *Torres et al.*, 2002; *Fromm and Servranckx*, 2003; *Damoah et al.*, 2004] or volcano eruptions [e.g., *Krotkov et al.*, 1999] have been detected and analyzed with the TOMS Aerosol Index. As for a practical application, the performance of an operational daily dust forecast model initialized by TOMS AI data [*Alpert et al.*, 2002] has also been tested by lidar measurements [*Kishcha et al.*, 2005].

[7] The presence of absorbing aerosol, such as desert dust and biomass burning products, is detected from TOMS measurements, in terms of AI, using a spectral contrast method in a UV region where the ozone absorption is

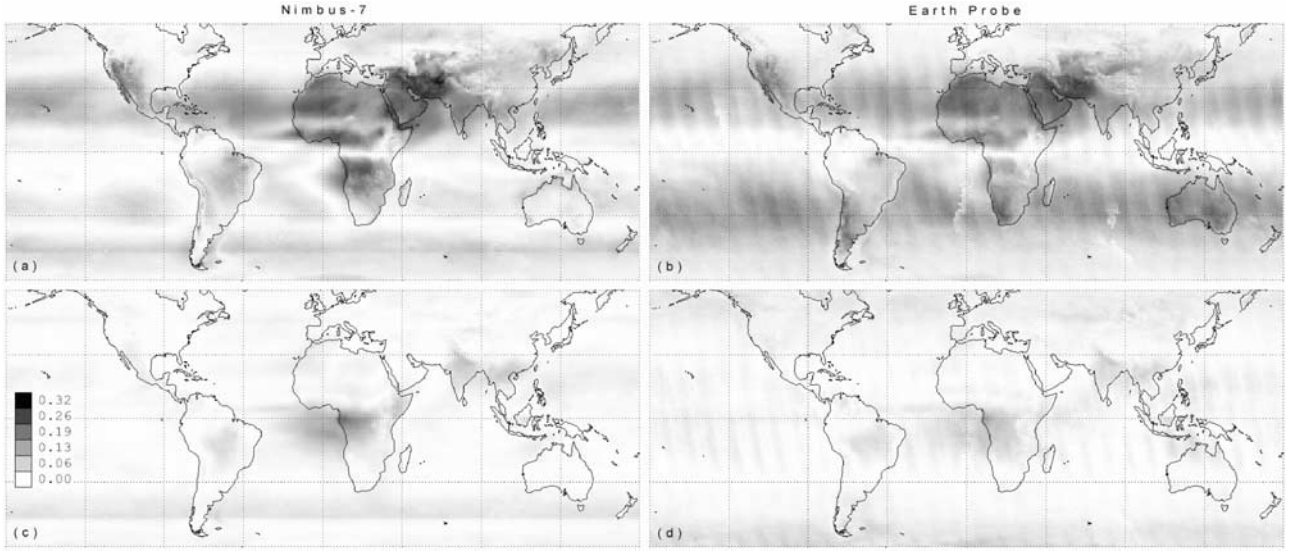

Figure 3. Geographic distribution of the spectral peak intensities indicated in Figure 2. (a) N7-AI, annual peak intensity. (b) EP-AI, annual peak intensity. (c) N7-AI, semi-annual peak intensity. (d) EP-AI, semi-annual peak intensity.

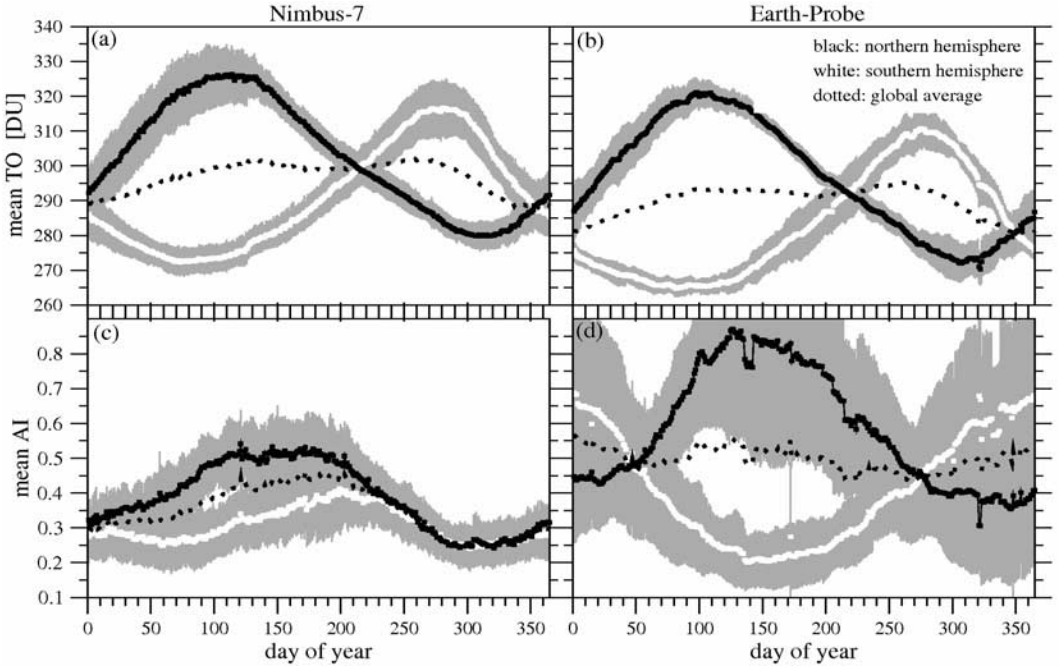

Figure 4. Annual cycle of daily mean total ozone (TO) and aerosol index (AI) averaged over 0.0° −60°N (northern hemisphere, black symbols) and 0.0° −60°S (southern hemisphere, white symbols): (a) N7-TO, (b) EP-TO, (c) N7-AI, and (d) EP-AI. Gray bands indicate one sigma standard deviations.

negligible [*Herman et al.*, 1997; *McPeters et al.*, 1998; *Torres et al.*, 1998; *Torres and Bhartia*, 1999], for a recent review see [*de Graaf et al.*, 2005]. The magnitude of the AI depends on aerosol optical depth, particle size distribution, optical properties and height above the surface of the absorbing aerosol layer, and on the viewing geometry. The wavelength definition of the TOMS AI has changed with the introduction of version 8 data in 2004, which has increased the sensitivity of the index by a factor of 1.5–2 [*de Graaf and Stammes*, 2005]. All AI data from 1978 to present have been reprocessed according to the new definition.

[8] Since version 8 data is relatively new, a systematic reevaluation has started only recently. As a first step of climatological description, it is quite plausible to check the behavior of global averages. In order to minimize the effects of instrumental errors at high solar zenith angles, the spatial averaging is restricted to latitudes between 60°S and 60°N covering ~87% of the earth surface. We have determined these near global daily average values for TO and AI with the results shown in Figure 1.

[9] The most conspicuous features for the mean aerosol signal (Figure 1c) are the pronounced excursion started in the year 2000, and the drastic change in the annual cycle in the Earth-Probe (EP) record relative to the seasonality of the 14-year Nimbus-7 (N7) record. A creeping trend was already identified in 2000 (http://toms.gsfc.nasa.gov/aerosols/aerosols.html), and it was reported as consequence of a wavelength dependent calibration drift resulting from changes in the optical properties of the front scan mirror of the EP instrument, which did not affect the total ozone calculation (P. K. Bhartia, personal communication, 2006). It is unclear if the absence of the expected annual cycle in the EP AI record is also associated with the suspected scan mirror anomaly.

2. Spectral Analysis, Annual Cycles

[10] In order to explore in more detail the apparent anomaly in EP-AI data, we have performed a detailed spectral analysis for each geographic location between 60°S and 60°N.

[11] We have implemented the Lomb periodogram algorithm [*Press et al.*, 1992] in order to properly treat missing days. Apart from the known high frequency peak of period 5.8 days in N7 data (caused by orbital overlaps), the two spectra computed separately from N7 and EP records for a given geographic location are similar (Figure 2). Since the EP record is shorter and the non-stationarity is more pronounced (see Figure 1c), a somewhat higher noise level and peak broadening are expected. Nevertheless, the main features are conserved for both satellite measurements: the dominant periodicities are semi-annual (Figures 2a and 2b) or annual (Figures 2c and 2d). (Quasi-biennial oscillations along the equator are also detected, but this is beyond the scope of the present analysis.)

[12] The spectral intensity of the semi-annual and annual components is estimated by integrating the grey areas in Figure 2. The geographic distribution of this parameter reveals significant differences between the N7 and EP data (see Figure 3). First of all, the N7 maps (Figures 3a and 3c) show a strong north-south asymmetry with a rather uneven distribution of spectral intensities. The presence of the southern stripe at around 45°S (especially in Figure 3c) suggests an artifact of instrumental origin. An amplification of the annual spectral peak amplitudes on the southern hemisphere is apparent for EP data (Figure 3b). Such an

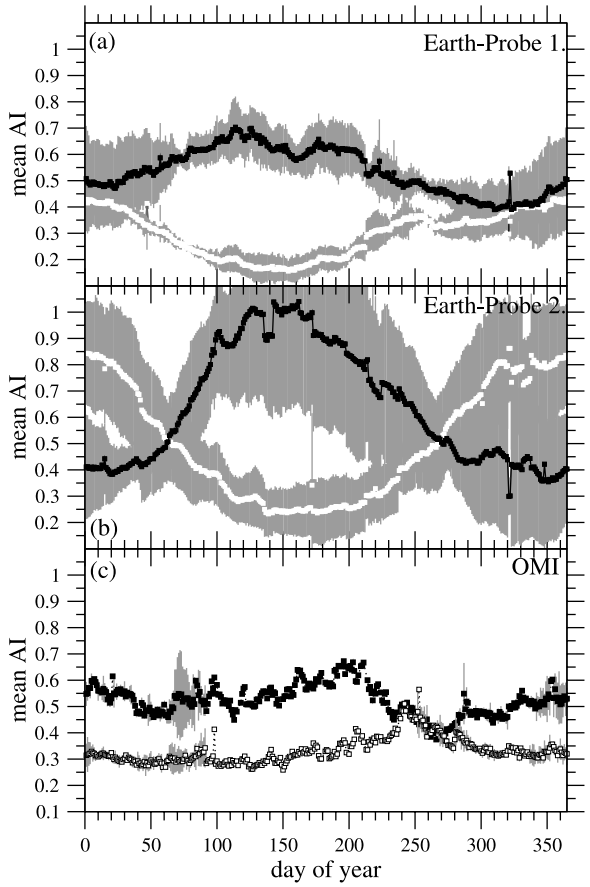

Figure 5. Annual cycle of daily mean aerosol index (AI) for the northern (black symbols) and for the southern (white symbols) hemispheres computed in three intervals, the scales are identical. (a) Earth-Probe data from 1-August-1996 to 31-July-2000. (b) Earth-Probe data from 1-August-2000 to 31-July-2005. (c) OMI data from July-2004 to April-2006.

increase is obvious also by comparing individual N7 and EP spectra at a given location, especially over Australia and below 20°S over South America. A further warning aspect of instrumental artifacts is the stripe of semi-annual peaks far in the south in Figure 3d, where a negligible aerosol signal is expected with much lower intensities than from African biomass burning.

[13] Figure 4 shows the daily mean TO and AI signals averaged separately over the northern (NH) and southern hemispheres (SH). The total ozone level (Figures 4a and 4b) has very similar annual cycles for both satellite records, the different amplitudes and phase shift explains the net periodicity shown in Figure 1a. The situation is quite different for the aerosol index values, where the two records are markedly different (Figures 4c and 4d).

[14] The annual cycle of the aerosol index for the two hemispheres as derived from Nimbus-7 TOMS measurements is shown in Figure 4c, produced by the combined effect of desert dust and carbonaceous aerosols. The NH AI signal is clearly dominated by the presence of mineral dust from world's major deserts augmented by the effect of carbonaceous aerosols from tropical and sub-tropical biomass burning. The SH shows a shorter aerosol season peaking in the fall, mainly the results of biomass burning in the Amazon Basin and Southern and Central Africa.

[15] The EP TOMS AI annual cycle (Figure 4d), on the other hand, is markedly different from the one shown by N7. The EP NH cycle retains the same general shape observed with N7, but the amplitude is about twice as large, probably the result of a calibration drift known to be affecting the sensor since about mid-2000. The EP SH seasonality does not show the spring maximum associated with the biomass burning activities. In the SH, the calibration drift effect seems to completely override the aerosol effect annual cycle, resulting in a seasonality closely associated with the sun's yearly cycle. The wide band of standard deviation around the mean EP-AI values (Figure 4d) indicates an enhanced noise level, which cannot be fully explained by the shorter record length (compare the TO signals in Figures 4a and 4b). Instrumental problems were detected in early 2001, and a warning was released that TOMS data past mid 2000 should not be used for trend analysis (http://toms.gsfc.nasa.gov/news/news.html). Examination of the single wavelength reflectivity data record shows that problems occurred during the first year after launch (J. Herman, personal communication, 2006).

[16] The temporal progression of the calibration drift can be appreciated by examining the EP-TOMS record split into two periods as shown in Figure 5. The period since launch (July 1996) thru July 2000 (Figure 5a), shows a NH cycle that closely resembles the N7 TOMS observed seasonality. The SH data, however, shows that even during the first few years after launch there were clear signs of calibration drift affecting the AI's magnitude and annual variability. The resulting seasonality over the second period (August 2000 – August 2005) depicted in Figure 5b, shows that the cali-

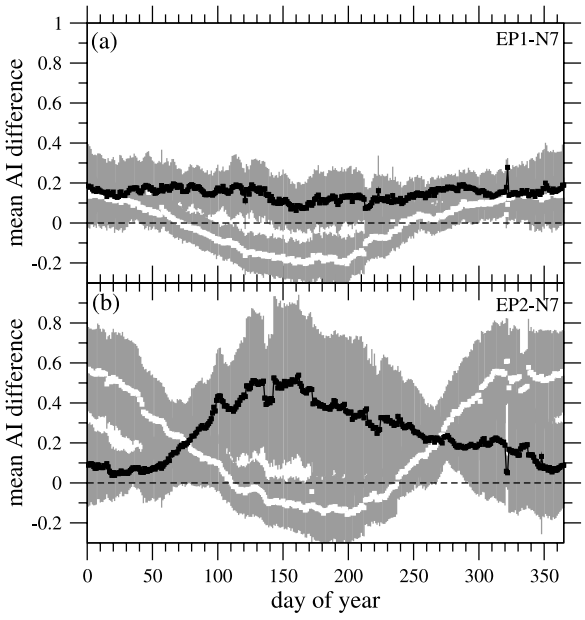

Figure 6. Difference of annual mean signals illustrating the calibration drift at EP-TOMS AI signals: (a) first half EP period (Figure 5a) minus N7 (Figure 4c) and (b) second half EP period (Figure 5b) minus N7 (Figure 4c). The notations are identical with Figures 4 and 5. Note that standard errors are obtained by means of the error propagation rule.

bration drift issue has begun to noticeably affect the NH, while the effect in the SH has considerably worsened. The return to the N7 TOMS-like yearly cycle in both hemispheres shown by the first year of OMI (Ozone Monitoring Instrument), Figure 5c, confirms the spurious nature of the EP TOMS AI temporal variability, especially after 2000. By taking out the aerosol related annual cycle, given the N7 record, from the EP data, the net calibration effect on the AI can be obtained as shown in Figure 6. The NH 1996–2000 record shows a small bias ($\sim$0.2) but not with a strong time dependence, while the 2000–2005 clearly shows a marked annual cycle associated with the sun's noontime zenith angle. In the SH, the calibration drift signal clearly intensifies from the first to the second period. The AI drift shown in Figure 6 is significantly larger than the AI precision for trend analysis estimated as 0.1. The calibration drift in AI units shown in Figure 6, can also be interpreted as percent reflectance change between the 331 and 360 nm channels by multiplying the AI numbers by 2.3.

[17] The comparison of Figure 5a with Figure 5b confirms that the amplification of the average AI value and noise level is escalated in the second period, after mid 2000. However, the hemispheric annual cycles are completely different from the N7 behavior (Figure 4c) already in the first EP period (Figure 5a). The near perfect reflection symmetry explains at least why the overall annual periodicity disappeared in the global EP-AI signal (Figure 1c).

3. Discussion

[18] The preceding analysis conclusively shows that the calibration drift of the EP-TOMS sensor begun early in the lifetime of the instrument, initially affecting mostly the Southern Hemisphere, and later propagating to the Northern Hemisphere. This is clearly illustrated by the difference in the average annual cycles calculated for the N7 (1978–1992) and the EP (1996–2000) sensors. A similar comparison for the period 2000–2005 shows that by mid-2000, about four years after launch, the calibration drift effect has propagated globally.

[19] The spurious nature of the EP-TOMS observed seasonality of the AI is confirmed by examining the first 18 months of AI data derived from observations by the OMI sensor on the Aura satellite. The OMI sensor shows a return to a seasonal pattern similar to the one observed by the N7 sensor.

[20] The instrumental nature of the hemispheric dependence of the calibration drift is difficult to understand. It can only be speculated that the observed effect is probably associated with angular effects resulting from the degradation of the scanning mirror. The actual optical interaction between the degrading scanning mirror and the incident light responsible for the hemispheric difference in the outset of the effect is out of the scope of this paper.

[21] The observed calibration drift in AI units is significantly larger than 0.1 which is the estimated precision for trend analyses. Therefore, extreme care should be exercised in the interpretation of the magnitude of the EP-TOMS AI and its temporal variabiliy. The quantitative use of the EP-TOMS AI after July 2000 as a proxy of aerosol related parameters should be avoided since large errors are likely to affect the results of those types of analysis.

[22] **Acknowledgments.** This work was partially supported by the Hungarian Science Foundation (OTKA) under grants T047233 and TS044839. IMJ thanks the Hungarian Academy of Sciences for a János Bolyai research scholarship.

References

Alpert, P., S. O. Krichak, M. Tsidulko, H. Shafir, and J. H. Joseph (2002), A dust prediction system with TOMS initialization, *Mon. Weather Rev.*, *130*, 2335–2345.

Damoah, R., N. Spichtinger, C. Forster, P. James, I. Mattis, U. Wandinger, S. Beirle, T. Wagner, and A. Stohl (2004), Around the world in 17 days hemispheric-scale transport of forest fire smoke from Russia in May 2003, *Atmos. Chem. Phys.*, *4*, 1311–1321.

de Graaf, M., and P. Stammes (2005), SCIAMACHY Absorbing Aerosol Index calibration issues and global results from 2002–2004, *Atmos. Chem. Phys.*, *5*, 2385–2394.

de Graaf, M., P. Stammes, O. Torres, and R. B. A. Koelemeijer (2005), Absorbing Aerosol Index: Sensitivity analysis, application to GOME and comparison with TOMS, *J. Geophys. Res.*, *110*, D01201, doi:10.1029/2004JD005178.

Fromm, M. D., and R. Servranckx (2003), Transport of forest fire smoke above the tropopause by supercell convection, *Geophys. Res. Lett.*, *30*(10), 1542, doi:10.1029/2002GL016820.

Herman, J. R., P. K. Bhartia, O. Torres, C. Hsu, C. Seftor, and E. Celarier (1997), Global distribution of UV-absorbing aerosols from Nimbus 7/TOMS data, *J. Geophys. Res.*, *102*, 16,911–16,922.

Hsu, N. C., J. Herman, J. Gleason, O. Torres, and C. Seftor (1999), Satellite detection of smoke aerosols over a snow/ice surface by TOMS, *Geophys. Res. Lett.*, *26*, 1165–1168.

Israelevich, P. L., Z. Levin, J. H. Joseph, and E. Ganor (2002), Desert aerosol transport in the Mediterranean region as inferred from the TOMS aerosol index, *J. Geophys. Res.*, *107*(D21), 4572, doi:10.1029/2001JD002011.

Kishcha, P., F. Barnaba, G. P. Gobbi, P. Alpert, A. Shtivelman, S. O. Krichak, and J. H. Joseph (2005), Vertical distribution of Saharan dust over Rome (Italy): Comparison between 3-year model predictions and lidar soundings, *J. Geophys. Res.*, *110*, D06208, doi:10.1029/2004JD005480.

Krotkov, N. A., O. Torres, C. Seftor, A. J. Krueger, A. Kostinski, W. I. Rose, G. J. S. Bluth, D. Schneider, and S. J. Schaefer (1999), Comparison of TOMS and AVHRR volcanic ash retrievals from the August 1992 eruption of Mt. Spurr, *Geophys. Res. Lett.*, *26*, 455–458.

McPeters, R., et al. (1998), Earth Probe Total Ozone Mapping Spectrometer (TOMS) data product users guide, *NASA Tech. Pap.*, *NASA/TP1998206895*.

Press, W. H., S. A. Teukolsky, W. T. Vetterling, and B. P. Flannery (1992), *Numerical Recipes in C*, Cambridge Univ. Press, New York.

Prospero, J. M., P. Ginoux, O. Torres, S. E. Nicholson, and T. E. Gill (2002), Environmental characterization of global sources of atmospheric soil dust identified with the NIMBUS 7 Total Ozone Mapping Spectrometer (TOMS) absorbing aerosol product, *Rev. Geophys.*, *40*(1), 1002, doi:10.1029/2000RG000095.

Torres, O., and P. K. Bhartia (1999), Impact of tropospheric aerosol absorption on ozone retrieval from backscattered ultraviolet measurements, *J. Geophys. Res.*, *104*, 21,569–21,577.

Torres, O., P. K. Bhartia, J. R. Herman, and Z. Ahmad (1998), Derivation of aerosol properties from satellite measurements of backscattered ultraviolet radiation: Theoretical basis, *J. Geophys. Res.*, *103*, 17,099–17,110.

Torres, O., P. K. Bhartia, J. R. Herman, A. Sinyuk, and B. Holben (2002), A long term record of aerosol optical thickness from TOMS observations and comparison to AERONET measurements, *J. Atmos. Sci.*, *59*, 398–413.

I. M. Jánosi and P. Kiss, Department of Physics of Complex Systems, Loránd Eötvös University, P.O. Box 32, H-1518 Budapest, Hungary. (janosi@lecso.elte.hu)

O. Torres, NASA GSFC, Code 613.3, Greenbelt, MD 20771, USA. (torres@qhearts.gsfc.nasa.gov)